Final version

Oscillatory flow and temperature fields in an open tube with temperature difference across the ends

T.R. Ashwin[a], **G.S.V.L. Narasimham**[a,*], **Subhash Jacob**[b]

[a]**Department of Mechanical Engineering**

[b]**Centre for Cryogenic Technology**

Indian Institute of Science, Bangalore 560012, India

Abbreviated title: Oscillating flow in a tube

Abstract: The oscillating flow and temperature field in an open tube subjected to cryogenic temperature at the cold end and ambient temperature at the hot end is studied numerically. The flow is driven by a time-wise sinusoidally varying pressure at the cold end. The conjugate problem takes into account the interaction of oscillatory flow with the heat conduction in the tube wall. The full set of compressible flow equations with axisymmetry assumption are solved with a pressure correction algorithm. Parametric studies are conducted with frequencies of 5-15 Hz, with one end maintained at 100 K and other end at 300 K. The flow and temperature distributions and the cooldown characteristics are obtained. The frequency and pressure amplitude have negligible effect on the time averaged Nusselt number. Pressure amplitude is an important factor determining the enthalpy flow through the solid wall. The frequency of operation has considerable effect on penetration of temperature into the tube. The density variation has strong influence on property profiles during cooldown. The present study is expected to be of interest in applications such as pulse tube refrigerators and other cryocoolers, where oscillatory flows occur in open tubes.

Keywords: Pulsating flow, Pulse tube, Heat transfer, Laminar, Circular tube, Conjugate convection.

∗:Corresponding author. Telephone: +91-80-22932971, Fax: +91-80-23600648

Email address: mecgsvln@mecheng.iisc.ernet.in (Narasimham, G.S.V.L)

Nomenclature

c_p	constant pressure specific heat	$(\mathrm{J\,kg^{-1}\,K^{-1}})$
D,d	diameter	(m)
$\dot{E}$	enthalpy flow	(W)
Ec	Eckert number, $v_\mathrm{c}^2/c_{\mathrm{p,c}}\,T_\mathrm{c}$	dimensionless
f	frequency	(Hz)
g	acceleration due to gravity	$(\mathrm{m\,s^{-2}})$
H	length of tube	(m)
h	heat transfer coefficient	$(\mathrm{W\,m^{-2}\,K^{-1}})$
k	thermal conductivity	$(\mathrm{W\,m^{-1}\,K^{-1}})$
L	length	m
$\dot{M}$	mass flow rate	$\mathrm{kg\,s^{-1}}$
Nu	Nusselt number, $h\,R_\mathrm{i}/k$	dimensionless
p	pressure	(Pa)
Pr	Prandtl number, $\mu\,c_\mathrm{p}/k$	dimensionless
R	radius	(m)
Re	Reynolds number, $\omega R_\mathrm{i}^2\,\rho/\mu$	dimensionless
T	temperature	(K)
t	time	(s)
v	velocity	$(\mathrm{m\,s^{-1}})$

Greek Symbols

ΔT_c	characteristic temperature difference	K
γ	ratio of specific heats	dimensionless
ϵ	overheat ratio	dimensionless
μ	dynamic viscosity	$(\mathrm{kg\,m^{-1}\,s^{-1}})$
ν	kinematic viscosity	$(\mathrm{m^2\,s^{-1}})$
ρ	density	$(\mathrm{kg\,m^{-3}})$
ω	angular frequency	$(\mathrm{rad\,s^{-1}})$

Subscripts

a	amplitude
av	average
c	characteristic
e	evaporator or cold
f	fluid region
h	hot or ambient
i	inner
o	outer, charge pressure
p	time period
r	radial direction
s	solid region
w	wall
z	axial direction

Superscript

*	dimensionless quantity

1 Introduction

Oscillating flow through passages like pipes and conduits is of interest in biological applications in relation to blood flow, industrial heat exchangers, manifolds, combustion and regenerators of Stirling and pulse tube cryocoolers. In the studies aimed at determining the heat transfer and friction between the wall and oscillating flow, the pulsatile flow field is assumed to consist of a steady Poiseuille flow part and a purely oscillatory part. Such a flow could enhance heat transfer by breaking down the boundary layer. In other words, the pulsations can have considerable effect on the rate of heat transfer and thermal resistance due to the alteration of thickness of the thermal boundary layer [1]. The flow and temperature distributions that occur in oscillatory flow in a tube with the end portions of the tube maintained at different temperatures is of interest in pulse tube refrigerators. The present study is motivated by such an application. Due to the nature of the problem and the large temperature differences that exist, the problem is analyzed using the full set of compressible flow governing equations with the assumption of axis symmetry.

Faghri et al. [2] reported a study on the heat transfer from a cylindrical pipe where periodic flow is superimposed on a fully developed steady laminar flow. It was shown that the interaction between velocity and temperature pulsations generates an extra diffusivity akin to eddy diffusivity, contributing to larger heat transfer rates.

There are other numerical investigations such as those of Cho et al. [3] which focused attention on heat transfer characteristics of a pulsating flow in a pipe. Using unsteady boundary-layer equations, Cho et al. [3] found that the time-mean axial velocity profiles and the Nusselt number were largely unaffected by the changes in frequency parameter and amplitude of oscillation. The skin friction was found to be greater than that of steady flow. The influence of oscillation on skin friction is appreciable both in terms of magnitude and phase relation.

Amir et al. [4] presented a correlation for the prediction of the heat transfer coefficient in a heating process for steady and pulsating flow of air through a circular pipe. The pulsating frequency is between 5 and 60 Hz and a combined dimensionless number composed of the Reynolds number and a dimensionless flow frequency was used to correlate thermal behavior with flow parameters. When this number was below 2.1×10^5, there was no significant improvement in heat transfer. Similar work was reported by Chattopadhyay et al. [5] for simultaneously developing pulsating incompressible laminar flow in a pipe with constant wall temperature. The analysis proved that pulsation has a negligible effect on time-averaged heat transfer. Moschandreou et al. [6] reported that the rate of heat transfer is not significantly affected when the frequency is very low or very high, while Guo et al. [7] reported that heat transfer augmentation occurs at large amplitudes of oscillation. For turbulent pulsating flow, Wang [8] found that there exists an optimum Womersley number at which heat transfer is enhanced. Heat transfer characteristics of pulsating turbulent air flow in a pipe heated at uniform heat flux were experimentally investigated [9]. The results show that the Nusselt number is strongly affected by pulsation frequency, the relative Nusselt number increasing or decreasing depending on the frequency range. Zhao et al. [10] presented a heat transfer correlation in terms of the kinetic Reynolds number, dimensionless amplitude of oscillation, length-to-diameter ratio and the Prandtl number. Khabakhpasheva et al. [11] experimentally observed considerable phase shift between the velocity and pressure gradient in pulsating flows of viscoelastic fluids.

Hemida et al. [12] studied the pulsation effect on heat transfer in laminar incompressible flow in a duct for both thermally fully developed and developing conditions. The results show that the pulsation has negligible role in fully developed region but it has greater sensitivity in thermally developing region. For isothermal and isoflux boundary conditions, the effect

of pulsation on the time average heat transfer coefficient tends to be negative, but remains relatively small. But non-linear boundary conditions (e.g. radiation and natural convection) combined with pulsation resulted in a noticeable enhancement of the time average Nusselt number.

Other studies on pulsating turbulent flows include those of Li and Xu [13], Pascale et al. [14] and He et al. [15].

From the literature, it can be seen that pulsating gas flow in open tubes subjected to end-to-end temperature difference and its interaction with the tube wall has not received attention. Such flows find practical application in various cryocoolers and other thermal systems. In an earlier paper, the present authors reported a numerical simulation for the complete pulse tube refrigerator operating high frequencies [16]. The present paper is motivated by the need for a detailed study of the pulse tube for systems in the frequency range 5-15 Hz.

2 Formulation

2.1 Geometry

Fig. 1 shows the physical model and coordinate system. Cylindrical polar coordinate system is chosen with the assumption of axisymmetric flow and temperature distributions. The model consists of a cylindrical pipe with finite wall thickness and both the ends open. The flow and temperature distributions are assumed to be axisymmetric. The r-axis is perpendicular to the vertical axis and points outwards in a radial direction. The positive direction of the z-axis coincides with the vertical axis and points upwards. The gravity vector is parallel to the z-axis and acts vertically downwards. The portions of the tube beyond the open ends belong to the cold and warm heat exchangers of a pulse tube refrigerator. Thus the working medium when

entering one of the ends does so at a cryogenic temperature T_{e}. Similarly the working medium entering the other end of the tube is at a higher temperature T_{h}. The oscillating flow in the tube is driven by a sinusoidally varying pressure at the cold end of the tube. Since the so called DC component is absent, the fluid flow during a cycle takes place partly into and partly out of the tube at either end. The height of the tube and the inner and outer radii are H, R_{i} and R_{o}, respectively. Clearly the wall thickness δ_{w} is $R_{\mathrm{o}} - R_{\mathrm{i}}$. The oscillating heat transfer between the wall and the gas is taken into account through the coupling between the fluid and the solid at the interface. The annular surfaces of the solid at the tube ends are assumed to be insulated.

2.2 Non-dimensionalisation

The characteristic length L_{c} is taken as the inner radius R_{i} of the tube and the characteristic temperature T_{c} as the hot heat exchanger temperature T_{h}, which is the ambient temperature. The geometrical parameters of the problem are the dimensionless inner radius R_{i}^* of the tube, dimensionless height H^* and the dimensionless wall thickness δ_{w}^*. The characteristic density ρ_{c} corresponds to the state of helium at the charge pressure p_{o} and ambient temperature $T_{\mathrm{h}} = T_{\mathrm{c}}$. The characteristic thermal conductivity, specific heat and dynamic viscosity of the working medium, i.e. helium gas, correspond to T_{c} and are denoted respectively k_{c}, $c_{\mathrm{p,c}}$ and μ_{c}. The dimensionless temperature T^* is $(T - T_{\mathrm{c}})/\Delta T_{\mathrm{c}}$ where ΔT_{c} is $T_{\mathrm{h}} - T_{\mathrm{e}}$. The quantity $\epsilon = \Delta T_{\mathrm{c}}/T_{\mathrm{c}}$ is the overheat ratio. The characteristic pressure is p_{c} is taken as $\rho_{\mathrm{c}} v_{\mathrm{c}}^2$ where v_{c}, the characteristic velocity, is taken as ωL_{c}. The time is non-dimensionalised with the time period of the oscillation $1/\omega$. Thus the dimensionless time period t_{p}^* is 2π.

The dimensionless quantities are defined as:

$$t^* = t\omega,\ r^* = \frac{r}{L_\mathrm{c}},\ z^* = \frac{z}{L_\mathrm{c}},\ L_\mathrm{c} = R_\mathrm{i}$$
$$v_\mathrm{r}^* = \frac{v_\mathrm{r}}{v_\mathrm{c}},\ v_\mathrm{z}^* = \frac{v_\mathrm{z}}{v_\mathrm{c}},\ p^* = \frac{p}{\rho_\mathrm{c} v_\mathrm{c}^2},\ v_\mathrm{c} = \omega L_\mathrm{c}$$
$$T^* = \frac{T - T_\mathrm{c}}{\Delta T_\mathrm{c}},\ \epsilon = \frac{\Delta T_\mathrm{c}}{T_\mathrm{c}},\ \Delta T_\mathrm{c} = T_\mathrm{h} - T_\mathrm{e},\ T_\mathrm{c} = T_\mathrm{h}$$
$$\rho^* = \frac{\rho}{\rho_\mathrm{c}},\ c_\mathrm{p}^* = \frac{c_\mathrm{p}}{c_\mathrm{p,c}},\ \mu^* = \frac{\mu}{\mu_\mathrm{c}},\ k^* = \frac{k}{k_\mathrm{c}}$$
$$Re = \frac{v_\mathrm{c} L_\mathrm{c} \rho_\mathrm{c}}{\mu_\mathrm{c}},\ Pr = \frac{\mu_\mathrm{c} c_\mathrm{p,c}}{k_\mathrm{c}},\ Ec = \frac{v_\mathrm{c}^2}{c_\mathrm{p,c} T_\mathrm{c}}$$
$$H^* = \frac{H}{L_\mathrm{c}},\ \delta_\mathrm{w}^* = \frac{\delta_\mathrm{w}}{L_\mathrm{c}}$$

The dimensionless outer radius is $R_\mathrm{o}^* = R_\mathrm{o}/L_\mathrm{c} = 1 + \delta_\mathrm{w}^*$ and the dimensionless charge pressure $p_\mathrm{o}^* = p_\mathrm{o}/(\rho_\mathrm{c} v_\mathrm{c}^2)$. The dimensionless properties should correspond to the fluid or solid depending upon the region under consideration, i.e. the working medium or wall. Thus the dimensionless ratios, namely, μ_f^*, $c_\mathrm{p,f}^*$ and k_f^*, the subscript 'f' denoting fluid, are assigned a value of unity in the fluid domain. In the solid region, the property values should correspond to those of the solid, namely, k_s^* and $c_\mathrm{s}^* = c_\mathrm{s}/c_\mathrm{p,c}$. In the numerical analysis, the solid is treated as a fluid of infinite viscosity.

2.3 Dimensionless governing equations

The dimensionless continuity, momentum and energy equations are as follows:

Continuity equation

$$\frac{\partial \rho^*}{\partial t^*} + \frac{1}{r^*}\frac{\partial}{\partial r^*}(r^* \rho^* v_\mathrm{r}^*) + \frac{\partial}{\partial z^*}(\rho^* v_\mathrm{z}^*) = 0 \tag{1}$$

Momentum equation in the radial direction

$$\frac{\partial}{\partial t^*}(\rho^* v_{\mathrm{r}}^*) + \frac{1}{r^*}\frac{\partial}{\partial r^*}(r^*\rho^* v_{\mathrm{r}}^* v_{\mathrm{r}}^*) + \frac{\partial}{\partial z}(\rho^* v_{\mathrm{z}}^* v_{\mathrm{r}}^*) = -\frac{\partial p^*}{\partial r^*} + \frac{1}{Re}\left[\frac{1}{r^*}\frac{\partial}{\partial r^*}\left(r^*\mu^*\frac{\partial v_{\mathrm{r}}^*}{\partial r^*}\right)\right.$$
$$\left. + \frac{\partial}{\partial z^*}\left(\mu_*\frac{\partial v_{\mathrm{r}}^*}{\partial z^*}\right)\right] + S_{\mathrm{r}} \tag{2}$$

Momentum equation in axial direction

$$\frac{\partial}{\partial t^*}(\rho^* v_{\mathrm{z}}^*) + \frac{1}{r^*}\frac{\partial}{\partial r^*}(r^*\rho^* v_{\mathrm{r}}^* v_{\mathrm{z}}^*) + \frac{\partial}{\partial z^*}(r^*\rho^* v_{\mathrm{z}}^* v_{\mathrm{z}}^*) = -\frac{\partial p^*}{\partial z^*} + \frac{1}{Re}\left[\frac{1}{r^*}\frac{\partial}{\partial r^*}\left(r^*\mu^*\frac{\partial v_{\mathrm{z}}^*}{\partial r^*}\right)\right.$$
$$\left. + \frac{\partial}{\partial z^*}\left(\mu^*\frac{\partial v_{\mathrm{z}}^*}{\partial z^*}\right)\right] + S_{\mathrm{z}} \tag{3}$$

Energy equation

$$\frac{\partial}{\partial t^*}(\rho^* T^*) + \frac{1}{r^*}\frac{\partial}{\partial r^*}(\rho^* r^* v_{\mathrm{r}}^* T^*) + \frac{\partial}{\partial z^*}(\rho^* v_z^* T^*) = \frac{1}{RePr}\left[\frac{1}{r^*}\frac{\partial}{\partial r^*}\left(\frac{k^*}{c_{\mathrm{p}}^*}r^*\frac{\partial T^*}{\partial r^*}\right)\right.$$
$$\left. + \frac{\partial}{\partial z^*}\left(\frac{k^*}{c_{\mathrm{p}}^*}\frac{\partial T^*}{\partial z^*}\right)\right] + \frac{Ec}{c_{\mathrm{p}}^*\,\epsilon}\frac{Dp^*}{Dt^*} \tag{4}$$

Equation of state

$$p^* = \frac{1}{Ec}\,\rho^*\,\frac{\gamma - 1}{\gamma}(T^*\,\epsilon + 1) \tag{5}$$

The momentum source terms are given by:

$$S_{\mathrm{r}} = \frac{1}{Re}\left[\frac{\partial}{\partial z^*}\left(\mu^*\frac{\partial v_{\mathrm{z}}^*}{\partial r^*}\right) + \frac{1}{r^*}\frac{\partial}{\partial r^*}\left(r^*\mu^*\frac{\partial v_{\mathrm{r}}^*}{\partial r^*}\right) - \frac{2\mu^* v_{\mathrm{r}}^*}{r^{*2}} - \frac{2}{3}\frac{\partial}{\partial r^*}\left(\mu^* D^*\right)\right] \tag{6}$$

$$S_{\mathrm{z}} = \frac{1}{Re}\left[\frac{\partial}{\partial z^*}\left(\mu_*\frac{\partial v_{\mathrm{z}}^*}{\partial z^*}\right) + \frac{1}{r^*}\frac{\partial}{\partial r^*}\left(r^*\mu^*\frac{\partial v_{\mathrm{r}}^*}{\partial z^*}\right) - \frac{2}{3}\frac{\partial}{\partial r^*}(\mu^* D^*)\right] \tag{7}$$

where the dimensionless divergence is given by:

$$D^* = \frac{1}{r^*}\frac{\partial}{\partial r^*}(r^* v_{\mathrm{r}}^*) + \frac{\partial v_{\mathrm{z}}^*}{\partial z^*}$$

The substantive derivative Dp^*/Dt^* is given by:

$$\frac{Dp^*}{Dt^*} = \frac{\partial p^*}{\partial t^*} + v_{\mathrm{r}}^*\frac{\partial p^*}{\partial r^*} + v_{\mathrm{z}}^*\frac{\partial p^*}{\partial z^*}$$

2.4 Nusselt number and enthalpy flow

The Nusselt number at any axial location on the fluid-solid interface and at any time is defined as

$$Nu_{\mathrm{z}} = \left[\frac{\partial T^*}{\partial r^*}\right]_{r^*=R_{\mathrm{i}}^*} \tag{8}$$

The Nusselt number Nu_{av} is the average of Nu_{z} over the length of the interface and one time period.

$$Nu_{\mathrm{av}} = \frac{1}{H^*\, t_{\mathrm{p}}^*} \int_0^{H^*} \int_0^{t_{\mathrm{p}}^*} Nu_{\mathrm{z}}\, dz\, dt \tag{9}$$

The enthalpy flow through any cross-section is calculated as:

$$\dot{E}_{\mathrm{av}} = \frac{1}{\pi\, R_{\mathrm{i}}^{*2}} \int_0^{R_{\mathrm{i}}^*} \rho^*\, v_z^* c_p^* T^* (2\pi\, r^* dr^*) \tag{10}$$

2.5 Initial and boundary conditions

It is assumed that at the beginning (i.e. $t^* = 0$), the geometry is under ambient condition and the system is filled with helium gas at the charge pressure. These conditions are taken as 300 K and 25 bar.

No-slip and zero mass permeability is assumed on the solid boundary in contact with the fluid. Oscillating pressure and zero radial velocity are prescribed at the cold end of the tube. At the hot end of the tube, zero streamwise derivative of the radial velocity is prescribed. The axial velocities at the inlet and outlet are calculated using the continuity equation. On the axis of the tube, zero cross-stream derivative of the axial velocity and zero radial velocity are imposed.

At the interface between the solid and the fluid, heat flux continuity and no temperature jump conditions should be satisfied. This is done through the harmonic mean thermal conductivity method [18]. At the cold end, the temperature condition is taken as the cold heat exchanger temperature when the flow takes place into the tube and as zero axial temperature gradient when the flow is out of the tube. Similar conditions are also applied at the hot end of the tube.

The initial and boundary conditions can be expressed as follows in dimensionless form:

At $t^* \leq 0$: $v_{\mathrm{r}}^* = v_{\mathrm{z}}^* = 0$, $T^* = 1$ and $p^* = p_{\mathrm{c}}/(\rho_{\mathrm{c}} v_{\mathrm{c}}^2)$ (throughout the computational domain). The quantity v_{c} is given by ωL_{c}.

$$
\begin{aligned}
& v_{\mathrm{r}}^*(0, z^*, t^*) = 0;\ v_{\mathrm{r}}^*(1, z^*, t^*) = 0;\ v_{\mathrm{r}}^*(r^*, 0, t^*) = 0; \\
& \frac{\partial v_{\mathrm{r}}^*}{\partial z^*}(r^*, H^*, t^*) = 0;\ \frac{\partial v_{\mathrm{z}}^*}{\partial r}(0, z^*, t^*) = 0
\end{aligned} \tag{11}
$$

The last relation states that the radial derivative of axial velocity is zero on the axis in view of the symmetry.

The boundary conditions for the temperature at the open ends can be expressed as follows:

$$
\begin{aligned}
& \text{If } v_{\mathrm{z}}^*(r^*, 0, t^*) \leq 0 \text{ then } \frac{\partial T^*}{\partial z^*}(r^*, 0, t^*) = 0 \\
& \text{If } v_{\mathrm{z}}^*(r^*, 0, t^*) > 0 \text{ then } T^*(r^*, 0, t^*) = -1.0 \\
& \text{If } v_{\mathrm{z}}^*(r^*, H^*, t^*) > 0 \text{ then } \frac{\partial T^*}{\partial z^*}(r^*, H^*, t^*) = 0 \\
& \text{If } v_{\mathrm{z}}^*(r^*, H^*, t^*) \leq 0 \text{ then } T^*(r^*, H^*, t^*) = 1.0
\end{aligned} \tag{12}
$$

At the interface:

$$
-k_{\mathrm{f}}^* \frac{\partial T_{\mathrm{f}}^*}{\partial r^*} = -k_{\mathrm{s}}^* \frac{\partial T_{\mathrm{s}}^*}{\partial r^*};\ T_{\mathrm{f}}^* = T_{\mathrm{s}}^* \tag{13}
$$

The pressure oscillation at the inlet of the pipe is:

$$
p^*(t^*) = p_{\mathrm{o}}^* + p_{\mathrm{a}}^* \sin(t^*) \tag{14}
$$

where p_o^* is the dimensionless charge pressure.

3 Numerical method

The governing equations are discretized on staggered mesh. Fig. 2 shows the nodalized representation of the quantities on a staggered mesh [17]. The pressure, density, temperature and gas properties are defined at the control volume nodes. The radial and axial velocities are defined at the faces of the control volumes, as shown. Velocities required elsewhere are obtained by linear interpolation with respect to the grid metrics. The algebraic transformation of Roberts [22] is used in the radial direction for obtaining finer mesh at the axis and the solid-fluid interface. The solution is obtained by the SIMPLEC algorithm of Van Doormal and Raithby [19]. The time derivatives are approximated by backward differences and the diffusive terms, by central differences. For convective terms, the third-order accurate HLPA (Hybrid Linear and Parabolic Approximation) scheme is Zhu [20] is employed due to its good transportive property, upwind bias and lower false diffusion. The discretized equations in five point stencil form are solved using the Modified Strongly Implicit Procedure of Schneider and Zedan [21]. This solver, though iterative in nature, achieves a high degree of implicitness, characteristic of direct methods. The time step depends on the frequency and pressure amplitude. Typically each time period is divided into 400-800 time steps. The solid region is considered as a fluid region with infinite viscosity and appropriate density, specific heat and thermal conductivity. Following startup, the system reaches a periodic state after a sufficient time has elapsed. The time marching is continued until periodic conditions are achieved. Sufficient number of global iterations are performed at each time step. During each global iteration, the velocities, pressure correction, temperature and density are determined by solving the discretized equations. Global iteration over each time step is continued until

the residuals for continuity and energy are better than 10^{-3}.

Grid dependency of the results is checked by varying the grid size in the axial and radial directions. The axial divisions are varied from 100 to 200 and the radial divisions in the fluid from 10-15, with three nodes deployed in the wall region. The area-average velocity is plotted for two cases at the middle cross-section in Fig. 3. The mesh with 100 axial divisions is found to perform almost similar to that with 200 divisions. Grid sensitivity tests are also conducted for various Reynolds numbers and the 15×100 grid is found to be adequate for the geometry selected.

4 Validation of the computer code

The present code is validated against the simulation of Chattopadhyay et al. [5]. For this purpose, the present code was modified to incorporate oscillating velocity and isothermal wall boundary conditions. The validation is conducted for a Reynolds number of 200, for various velocity amplitudes and for frequencies below 20 Hz. A mesh with 100 control volumes in the radial direction and 800 control volumes in the axial direction was chosen. The frequency is adjusted to match the Strouhal number chosen in the original work. The results of the validation study presented in Table 1 show a favourable agreement between the two studies.

5 Results and discussion

5.1 The effect of pressure amplitude

Figures 4 and 5 show the temperature and velocity distributions inside the tube for pressure amplitude of 50 Pa and 500 Pa after 66 seconds. At this time the flow reversal is about to take place inside the tube. The temperature for the most part of the tube is between 250 and 280

K, the initialization temperature being 300 K. This shows that the temperature at the cold end stars penetrating into the tube and a temperature gradient is being setup in the tube. With open ends, it can be observed that a small pressure oscillation at the inlet results in large axial velocity gradient. The pressure amplitudes are kept low in order to prevent smearing of the temperature profiles by the large axial velocities in the tube. Because of the onset of the flow reversal at this time the velocities in the tube are very small. The flow reversal is mostly confined to the central part of the tube. The flow pattern suggests that there is a possibility for the occurrence of eddy formation at the entrance and exit in the central part of the tube.

The axial variation of wall temperature for two pressure amplitudes is presented in Fig. 6 for the middle cross-section of the tube wall at the mid thickness after 167 seconds for a frequency of 15 Hz after attaining periodic conditions. The attainment of periodic conditions is ensured by plotting the temperature distribution for two successive time periods and by observing that there is no change in these profiles. The mid thickness wall temperature at the tube inlet for the two the cases are different. For the first case with 50 Pa pressure amplitude, the solid cold end temperature is 183.38 K where as in the second case, the same is 142.37 K at the cold end. The wall to gas temperature difference in these two cases are respectively 83.38 K and 42.37 K. The reason is traced to the fact that higher pressure amplitudes result in higher velocities and lower thermal boundary layer thickness. It is observed, however that that the hot end temperature of the tube wall does not change much with pressure amplitudes, the wall to gas temperature difference at the hot end being very small, typically, 10 K for the first case and 15 K for the second case. Thus higher pressure amplitude appears to be lowering the cold end temperature of the wall and maintaining more or less the same hot end temperature. This can also be verified from the Table 2 which shows higher energy flow through the solid wall as the pressure amplitude increases for a given frequency. This could be due to the higher

density of the fluid at the cold end and lower density at the hot end. Moving away from the cold end to the hot end, the disturbances decrease and the rate of temperature change also decreases (Fig. 6). From Table 3, it can also be seen that the values of the average Nusselt number are rather lower compared to incompressible flow [5] and do not change much with frequency of operation or pressure amplitude. It should be noted that both ends and outer surface of the tube are insulated and therefore there the only thermal interaction between the gas and solid is through the interface. This observation is analogous to that of Himadri et al. [5] for incompressible flow. It may be recalled here that the Nusselt number is based on the difference between the hot and cold end temperatures rather than the difference of the time-averaged interface and bulk fluid temperatures.

Fig. 7 shows the variation of space averaged Nusselt number and variation of velocity over one cycle after 167 seconds of operation from startup. The pressure amplitude is 50 Pa and the frequency is 15 Hz. The variation in the Nusslet number over a cycle is found to stabilize after attaining periodic condition. The value of Nusselt number increases and decreases during a cycle. The variation of the cross-section averaged velocity is also shown in this Figure. The variation in the Nusselt number follows the same pattern as that of the average velocity over one cycle.

The radial velocity corresponding to an instant is plotted against the axial velocity at the same instant in Fig. 8. The location of the monitoring point is at the mid radius and at the mid length of the tube, the frequency and amplitude being 15 Hz and 50 Pa. Since the curve closes on itself, it can be concluded that the cooldown phase is passed and the flow field has become fully periodic.

Fig. 9 shows the area-averaged axial velocity profiles after 6.66 seconds and 167 seconds of operation at the middle cross section of the tube. The observations are taken for a case

of 500 Pa amplitude and 15 Hz frequency. Though the shorter time and longer time profiles are similar in shape, the profile is found to shift downwards as the periodic state approaches. Although not shown here, such a marked shift is not observed between the shorter time and longer time temperature profiles. This can be due to the strong influence of density variation in the beginning of the operation. All the cases are initialized with ambient condition at the startup. The thermal effect of the cold end diffuses into the tube and causes a strong density variation influencing thereby the velocity profiles inside the tube. This kind of distortion has earlier been reported by the authors in a previous study on a pulse tube refrigerator at higher frequencies [16].

Fig. 10 shows the cooldown characteristics for 15 Hz frequency and 500 Pa pressure amplitude at the middle of the tube. The non dimensional temperature plotted is the area average over the cross-section. Time advancement is executed until the temperature variation of two consecutive cycle stabilizes. The best fit for the cooldown characteristic data in terms of dimensionless temperature and dimensionaless time, is given by:

$$\begin{aligned} T^* &= -8.08 \times 10^{-3} - 9.11 \times 10^{-5}\, t^* + 3.14 \times 10^{-8}\, t^{*2} - 6.32 \times 10^{-12}\, t^{*3} \\ &\quad +6.52 \times 10^{-16}\, t^{*4} - 3.27 \times 10^{-20}\, t^{*5} + 6.35 \times 10^{-25}\, t^{*6} \end{aligned} \tag{15}$$

The average absolute deviation for the above fit is 0.0072 and the multiple correlation is 0.976. The above equation is valid for the dimensionless time ranges presented in Fig. 10.

5.1.1 Effect of frequency

Fig. 11 shows the variation of temperature at the middle cross section of the tube over one cycle for frequencies of 10 Hz and 15 Hz. The different temperature scales for the lower and higher frequencies may be noted. The temperature is calculated as area weighted average. As

the frequency increases, the temperature penetration into the tube becomes deeper. The inlet temperature could cool the gas in the middle section up to an average value of 269 K with a temperature amplitude of 0.4 K. For frequency of 10 Hz the cross section temperature is average 295 K with a temperature amplitude of 0.8 K. From this, it can be observed that the temperature penetration increases with increase in frequency. For a pulse tube refrigerator, three fluid zones can be identified; a zone near the cold end, a central zone and a zone near the hot end. The mixing of gases of cold and hot zone will destroy the cooling effect. Higher frequency pulse tubes are likely to exhibit mixing of gases between the two end zones because of deeper temperature penetration. Thus the length to diameter ratio should be properly adjusted to prevent mixing of gases. The frequency of operation is also an important factor other than length to diameter ratio, in designing the pulse tube refrigerator [16].

Fig. 12 shows the temperature distribution of gas and solid for a particular instant. The observations are taken for a model working with frequency 10 Hz and 50 Pa amplitude. The figure shows a large temperature difference, amounting to 151 K, at the inlet of the tube. Proper meshing is important in this region to capture the large temperature gradient. The temperature differences decrease to a value of 10^{-3} at the exit. The energy transfer between the wall and the gas decreases with axial distance. The temperature difference at the cold end is the main source of pumping energy to the wall of the tube. Fig. 13 shows the heat transfer between the working gas and the wall at middle cross section of the tube after cooldown. The results indicate that the gas-wall heat transfer is higher for higher frequency systems. Detailed energy balance sheet is given in Table 2. The gas and solid enthalpy flow is calculated at the middle cross section (i.e. at $H/2$) and near the exit ($4H/3$) of the tube. The table shows that the heat transfer through the solid wall is negligible compared to the enthalpy flow through the gas. The difference in the cycle average enthalpy flow between the two cross sections is

found to be negligible.

5.2 Phase relationships

Fig. 14 shows the phase relationship between the temperature and mass flow rate at the middle cross-section of the tube after periodic condition is achieved for frequencies of 10 and 15 Hz. These are the area-averaged quantities over the cross-section. Such data is very important for designing devices like pulse tube refrigerator, since the heat released or absorbed directly depends on the phase relationship between the mass flow and the temperature. Assuming ideal gas relation, the enthalpy flow over a cycle can be written as:

$$\dot{E} = \frac{1}{t_{\mathrm{p}}} \oint_0^{t_{\mathrm{p}}} \dot{M} c_{\mathrm{p}} dt \tag{16}$$

It can be seen from Fig. 14 that temperature leads the mass flow rate for both the frequencies. The phase relationship between these quantities depends upon several factors like geometrical dimensions of the tube, the frequency and the pressure amplitude. Ideally the temperature should be in phase with the mass flow rate for maximum enthalpy flow rate.

5.3 Conclusions

The problem of oscillating flow inside an open tube with finite wall thickness, ambient to cryogenic temperature difference at the ends, driven by sinusoidal pressure variation at the cold end is studied numerically by solving the full set of compressible conservation equations with axisymmetry. Parametric studies are conducted with different pressure amplitudes and frequencies. The wall to gas temperature difference is maximum at the cold end and lowest at the hot end. As the pressure amplitude increases, the temperature difference between the wall and the fluid decreases due to mixing at the cold end. The temperature difference at the

hot end is less sensitive to the pressure amplitude. The frequency of operation is an important factor in determining the temperature penetration into the tube. This should be taken into account for designing devices like pulse tube refrigerators. There is a strong influence of temperature during cooldown which directly affects the property variations inside the tube. The pressure amplitude and the frequency have a negligible effect on the time averaged Nusselt number for the boundary conditions and geometry considered. The result is analogous to the previous findings for incompressible oscillatory flow. Data on the phase relationship between the temperature and mass flow rate is useful in designing devices like pulse tube refrigerators.

References

[1] E.G. Richardson, The transverse velocity gradient near the mouths of pipes in which an alternating or continuous flow of air is established, Proceedings of the Royal Society London, A42 (1929) 1-15.

[2] M. Faghri, K. Javdani, A. Faghri, Heat transfer with laminar pulsating flow in a pipe, Letters in Heat and Mass transfer 6 (1979) 259-270.

[3] H.W. Cho, J.M. Hyun, Numerical solutions of pulsating flow and heat transfer characterestics in a pipe, International Journal of Heat and Fluid Flow 11 (1990) 321-330.

[4] A.A. Al-Haddad, N. Al-Binally, Prediction of heat transfer coefficient in pulsating flow, International Journal of Heat and Fluid Flow 10 (1989) 131-133.

[5] H. Chattopadhyay, F. Durst, S. Ray, Analysis of heat transfer in simultaneously developing pulsating laminar flow in a pipe with constant wall temperature, International Communications in Heat and Mass Transfer 33 (2006) 475-481.

[6] T. Moschandreou, M. Zamir,Heat transfer in a tube with pulsating flow and constant heat flux, International Journal of Heat Mass Transfer, 40 (1997) 2461-2466.

[7] Z. Guo, H.J. Sung, Analysis of the Nusselt number in pulsating pipe flow, International Journal of Heat and Mass Transfer 40 (1997) 2486-2489.

[8] X. Wang, N. Zhang, Numerical analysis of heat transfer in pulsating turbulent flow in a pipe, International Journal of Heat and Mass Transfer 48 (2005) 3957-3970.

[9] A.M.E. Elshafei, M.S. Mohamed, H. Mansour, M. Sakr, Experimental study of heat transfer in pulsating turbulent flow in a pipe, International Journal of Heat and Fluid Flow 29 (2008) 1029-1038.

[10] T. Zhao, P. Cheng, A numerical solution of laminar forced convection in a heated pipe subjected to a reciprocating flow, International Journal of Heat and Mass Transfer 38 (1995) 3011-3022.

[11] E.M. Khabakhpasheva, V.I. Popov, A.N. Kekalov, E.S. Mikhailova, Pulsating flow of viscoelsatic fluids in tubes, Journal of Non-Newtonian Fluid Mechanics 33 (1989) 289-304

[12] H.N. Hemida, M.N. Sabry, A. Abdel-Rahim, H.Mansour, Theoretical analysis of heat transfer in laminar pulsating flow, International Journal of Heat and Mass Transfer 45 (2002) 1767-1780.

[13] Z.C. Li, L. Xu, Experimental investigation on the performances of gas flow in oscillating tube, Proceedings of the Twentieth International Cryogenic Engineering Conference, Beijing, China (2004) 257-260.

[14] P. Bouvier, P. Stouffs, J.-P. Bardon, Experimental study of heat transfer in oscillating flow, International Journal of Heat and Mass Transfer 48 (2005) 2473-2482.

[15] S. He, J.D. Jackson, An experimental study of pulsating turbulent flow in a pipe, European Journal of Mechanics B/Fluids 28 (2009) 309-320.

[16] T.R. Ashwin, G.S.V.L. Narasimham, S. Jacob, CFD analysis of high frequency miniature pulse tube refrigerators for space applications with thermal non-equilibrium model, Applied Thermal Engineering 30 (2010) 152-166.

[17] F.H. Harlow, J.E. Welch, Numerical calculation of time-dependent viscous incompressible flow of fluid with free surface, The Physics of Fluids 8 (1965) 2182-2189.

[18] S.V. Patankar, Numerical heat transfer and fluid flow, Series in Computational Methods in Mechanics and Thermal Sciences, Hemisphere Publishing Corporation (1980) Washington.

[19] J.P. Van Doormaal, G.D. Raithby, Enhancements of the SIMPLE method for predicting incompressible fluid flows, Numerical Heat Transfer 7 (1984) 147-163.

[20] J. Zhu, A low-diffusive and oscillation-free convection scheme, Communications in Applied Numerical Methods 7 (1991) 225-232.

[21] G.E. Schneider, M. Zedan, A modified strongly implicit procedure for the numerical solution of field problems, Numerical Heat Transfer 4 (1981) 1-19.

[22] G.O. Roberts, Computational meshes for boundary layer problems, Proceedings of the Second International Conference on Numerical Methods in Fluid Dynamics, Springer-Verlag Berlin (1971) 171-177.

Figure Captions

Fig.1 Physical model and coordinate system.

Fig.2 Location of variables in a staggered mesh.

Fig.3 Results of the grid sensitivity analysis.

Fig.4 Temperature and velocity profiles for 15 Hz frequency and p_a=50Pa after 66.66 seconds from startup.

Fig.5 Temperature and velocity profiles for 15 Hz frequency and p_a=500Pa after 66.66 seconds from startup.

Fig.6 Wall temperature distribution at two pressure amplitudes.

Fig.7 Variation of the area-averaged velocity at the mid-cross section and that of the wall Nusselt number over one cycle.

Fig.8 Plot of radial versus axial velocity at mid cross-section and mid radius over a cycle.

Fig.9 Time variation of area-averaged axial velocity at mid cross-section before and after stabilization.

Fig.10 Cooldown characteristics for a frequency of 15 Hz and a pressure amplitude of 500 Pa.

Fig.11 Time variation of area-averaged temperature for frequencies of 10 Hz and 15 Hz.

Fig.12 Axial temperature distribution of gas adjacent to the interface and that of the wall at mid thickness.

Fig.13 Time variation of the heat transfer between the gas and wall.

Fig.14 Phase relationship between the temperature and the mass flow rate at the middle of the tube. **(a)**Frequency 10Hz **(b)**Frequency 15Hz

List of Tables

Table 1: Results of the validation study

Velocity amplitude	Strouhal number St	Frequency f	Nu_{av} Chattopadhyay et al. [5]	Nu_{av} Present Model
0.2	5	8.95	0.96	0.99
0.2	10	17.90	0.96	0.97
0.5	10	17.90	0.96	1.01

Table 2: Energy balance for different cases

Case	Reynolds number (Re)	Time of operation (s)	Time average gas enthalpy at $\frac{1}{2}H$ ($\dot{E}_{\text{av}}$) (W)	Time average solid enthalpy at $\frac{1}{2}H$ ($\dot{E}_{\text{av}}$) (W)	Time average gas enthalpy at $\frac{3}{4}H$($\dot{E}_{\text{av}}$) (W)	Time average solid enthalpy at $\frac{3}{4}H$($\dot{E}_{\text{av}}$) (W)
Case 1	28.1	2501	1.42×10^5	1.59×10^{-1}	1.42×10^5	1.59×10^{-1}
Case 2	140.48	501	1.26×10^5	2.84×10^{-2}	1.26×10^5	2.84×10^{-2}
Case 3	140.48	501	1.39×10^5	2.19×10^{-1}	1.39×10^5	2.19×10^{-1}
Case 4	280.96	250.1	1.29×10^5	2.06×10^{-2}	1.29×10^5	2.06×10^{-2}
Case 5	421.45	167	1.75×10^5	3.56×10^{-2}	1.75×10^5	3.56×10^{-2}
Case 6	421.45	167	1.98×10^5	8.54×10^{-2}	1.98×10^5	8.54×10^{-2}

Table 3: Results of the parametric studies

Case no	Pressure amplitude p_{a} (Pa)	Frequency (f) (Hz)	Time of operation (s)	Time average Nusselt Number (Nu_{av})
Case 1	50	1	2501	1.18×10^{-1}
Case 2	50	5	501	1.33×10^{-1}
Case 3	500	5	501	1.35×10^{-1}
Case 4	50	10	250.1	1.49×10^{-1}
Case 5	50	15	167	1.77×10^{-1}
Case 6	500	15	167	1.00×10^{-1}

Figures

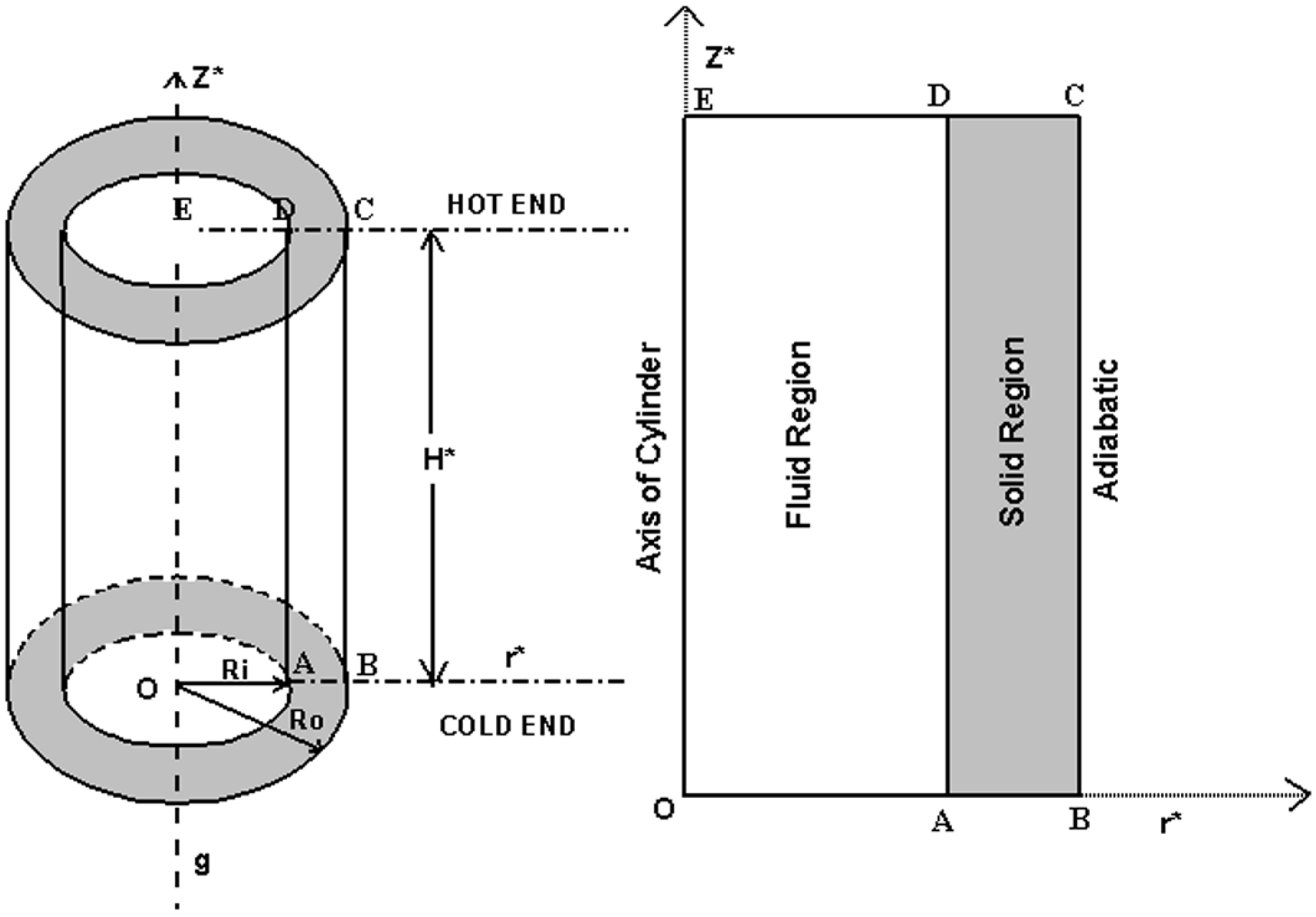

Figure 1:

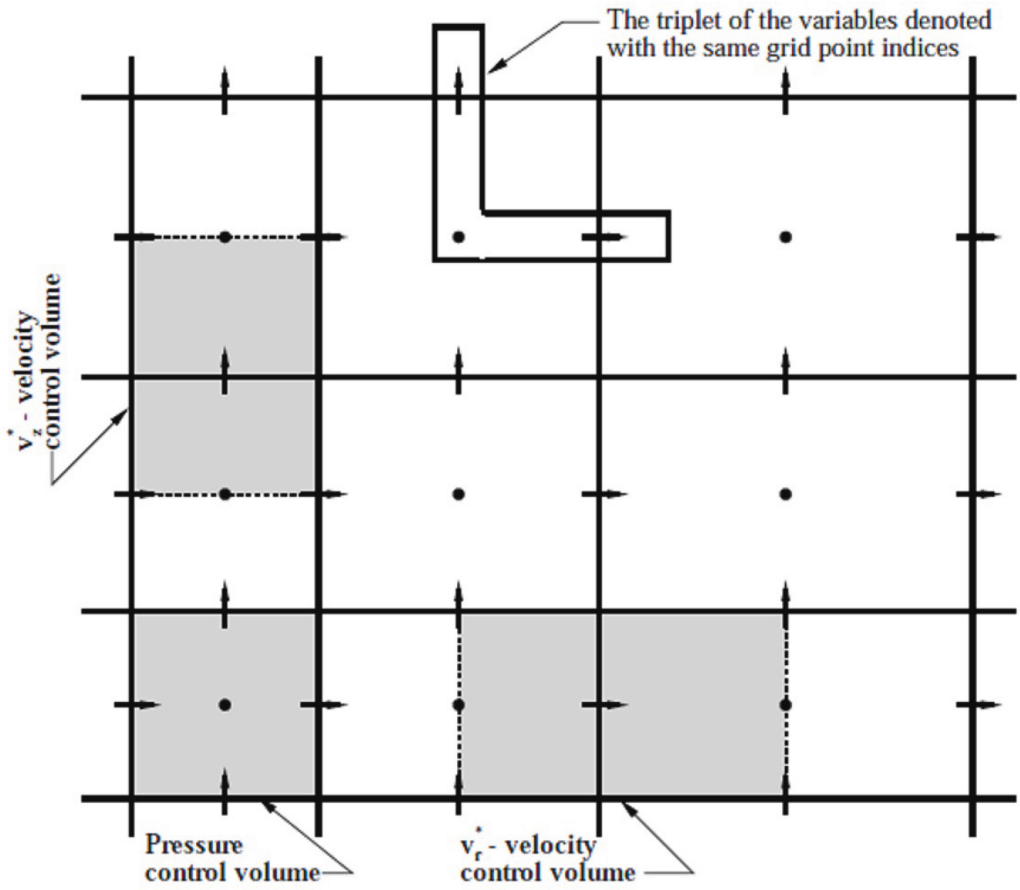
The triplet of the variables denoted
with the same grid point indices
v_z^* - velocity
control volume
Pressure
control volume
v_r^* - velocity
control volume

Figure 2:

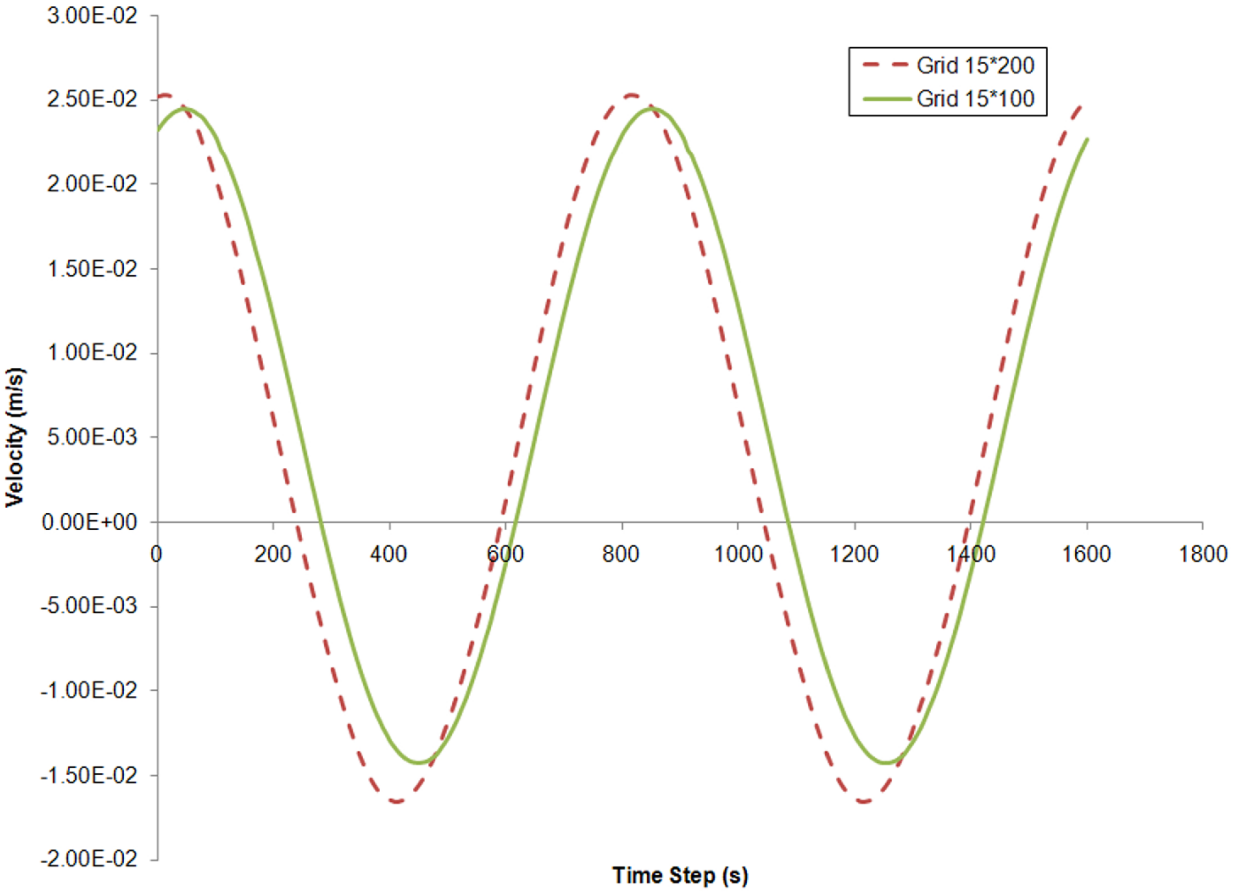
3.00E-02
2.50E-02
2.00E-02
1.50E-02
1.00E-02
5.00E-03
0.00E+00
-5.00E-03
-1.00E-02
-1.50E-02
-2.00E-02
Velocity (m/s)
0
200
400
600
800
1000
1200
1400
1600
1800
Time Step (s)
Grid 15*200
Grid 15*100

Figure 3:

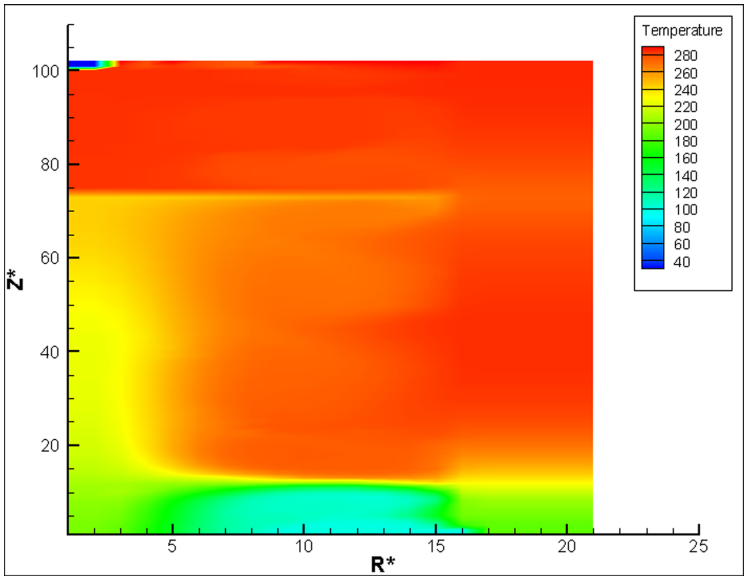
Temperature
280
260
240
220
200
180
160
140
120
100
80
60
40
100
80
60
40
20
Z*
5
10
15
20
25
R*

(a)

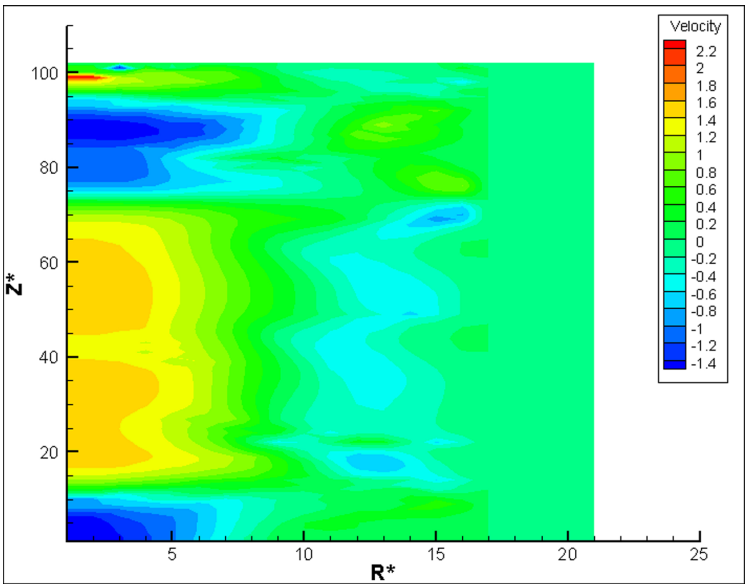
Velocity
2.2
2
1.8
1.6
1.4
1.2
1
0.8
0.6
0.4
0.2
0
-0.2
-0.4
-0.6
-0.8
-1
-1.2
-1.4
100
80
60
40
20
Z*
5
10
15
20
25
R*

(b)

Figure 4:

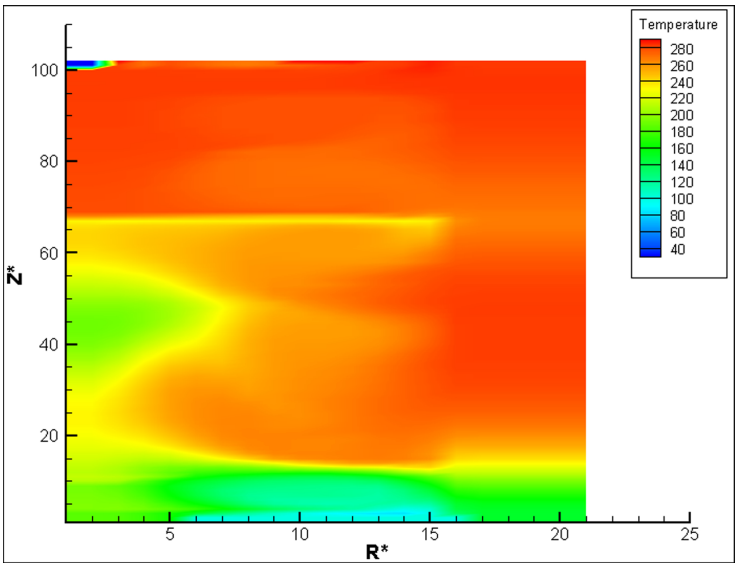
Temperature
280
260
240
220
200
180
160
140
120
100
80
60
40
Z*
R*
100
80
60
40
20
5
10
15
20
25

(a)

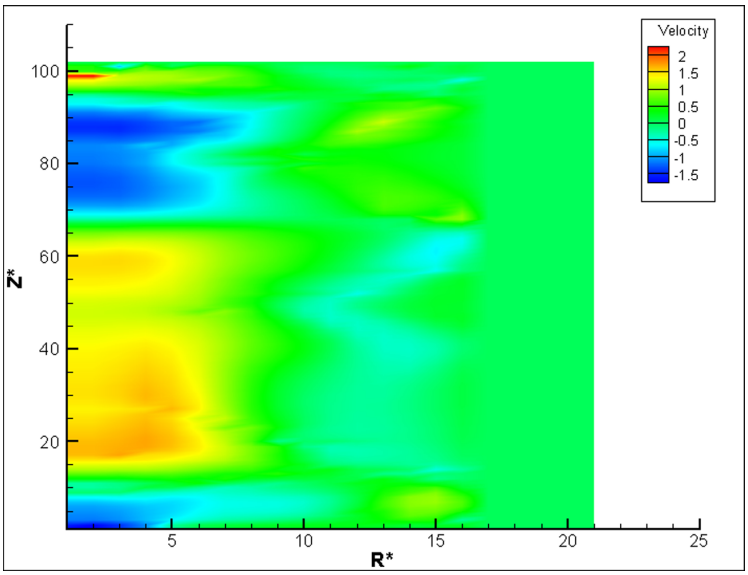
Velocity
2
1.5
1
0.5
0
-0.5
-1
-1.5
Z*
R*
100
80
60
40
20
5
10
15
20
25

(b)

Figure 5:

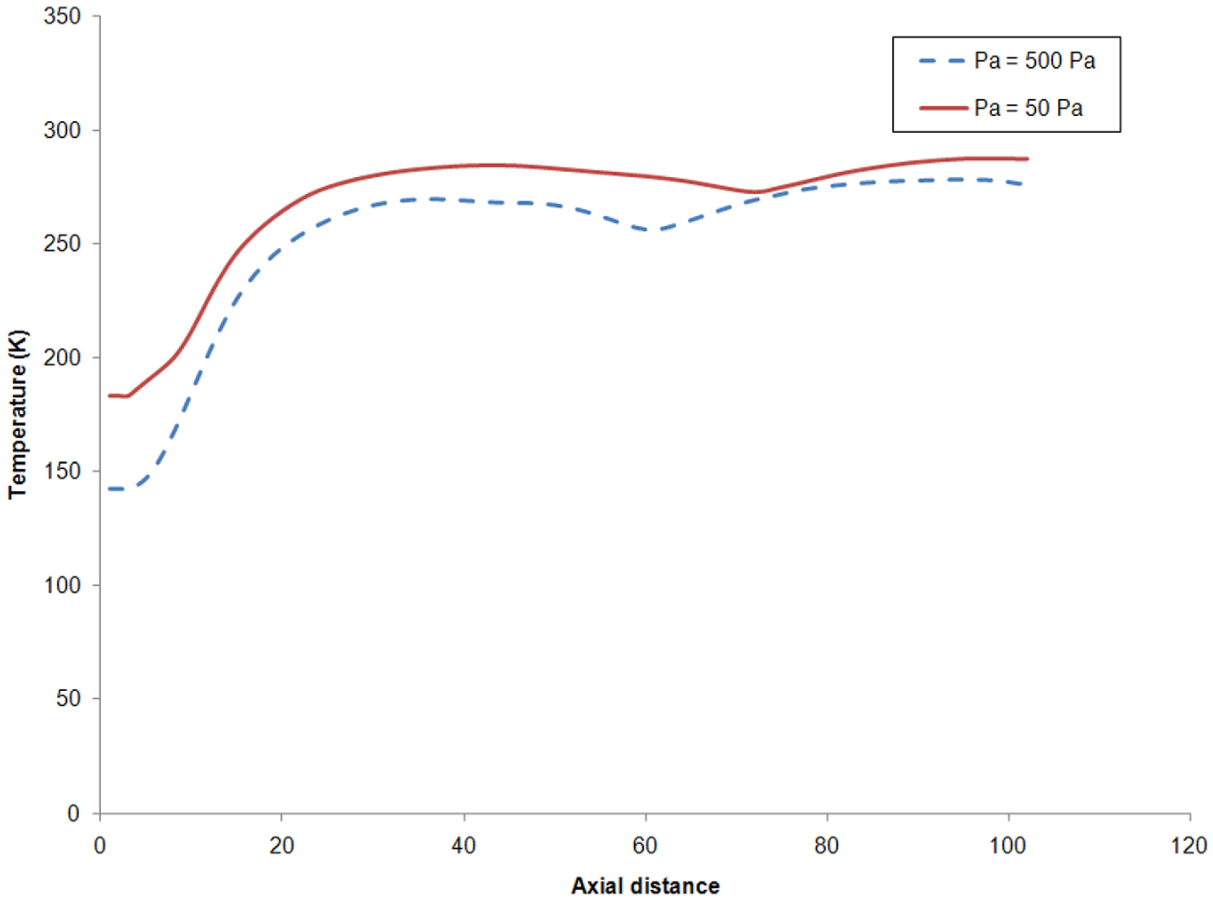
350
300
250
200
150
100
50
0
Temperature (K)
0
20
40
60
80
100
120
Axial distance
Pa = 500 Pa
Pa = 50 Pa

Figure 6:

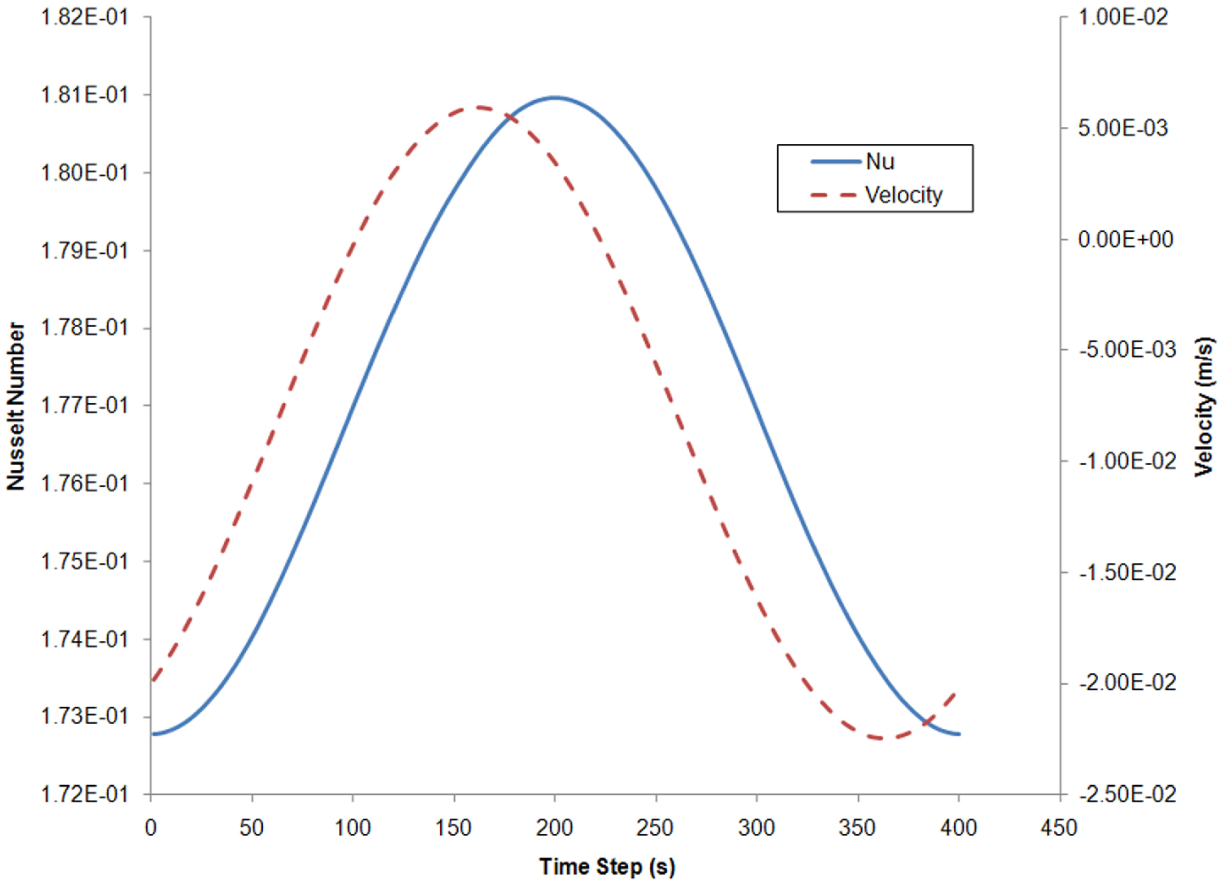
1.82E-01
1.81E-01
1.80E-01
1.79E-01
1.78E-01
1.77E-01
1.76E-01
1.75E-01
1.74E-01
1.73E-01
1.72E-01
Nusselt Number
1.00E-02
5.00E-03
0.00E+00
-5.00E-03
-1.00E-02
-1.50E-02
-2.00E-02
-2.50E-02
Velocity (m/s)
Nu
Velocity
0
50
100
150
200
250
300
350
400
450
Time Step (s)

Figure 7:

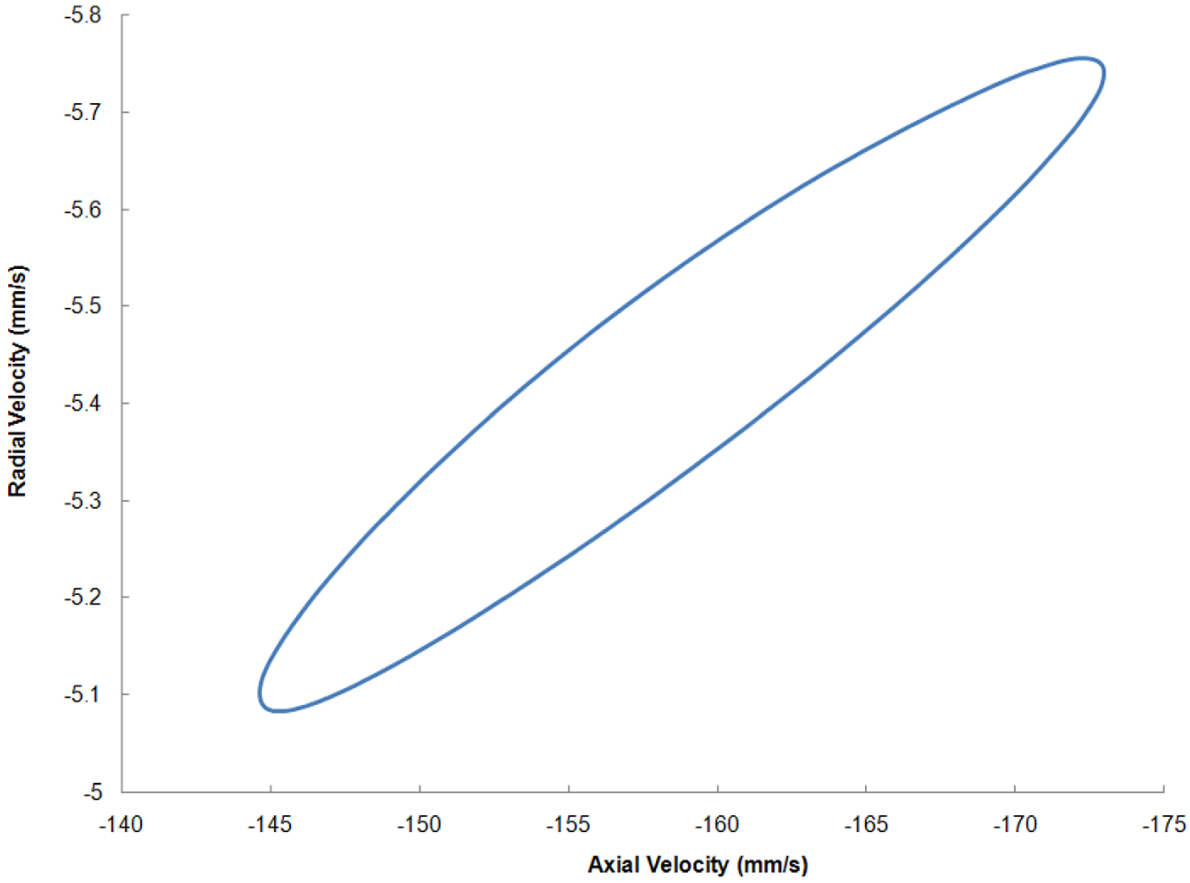
-5.8
-5.7
-5.6
-5.5
-5.4
-5.3
-5.2
-5.1
-5
Radial Velocity (mm/s)
-140
-145
-150
-155
-160
-165
-170
-175
Axial Velocity (mm/s)

Figure 8:

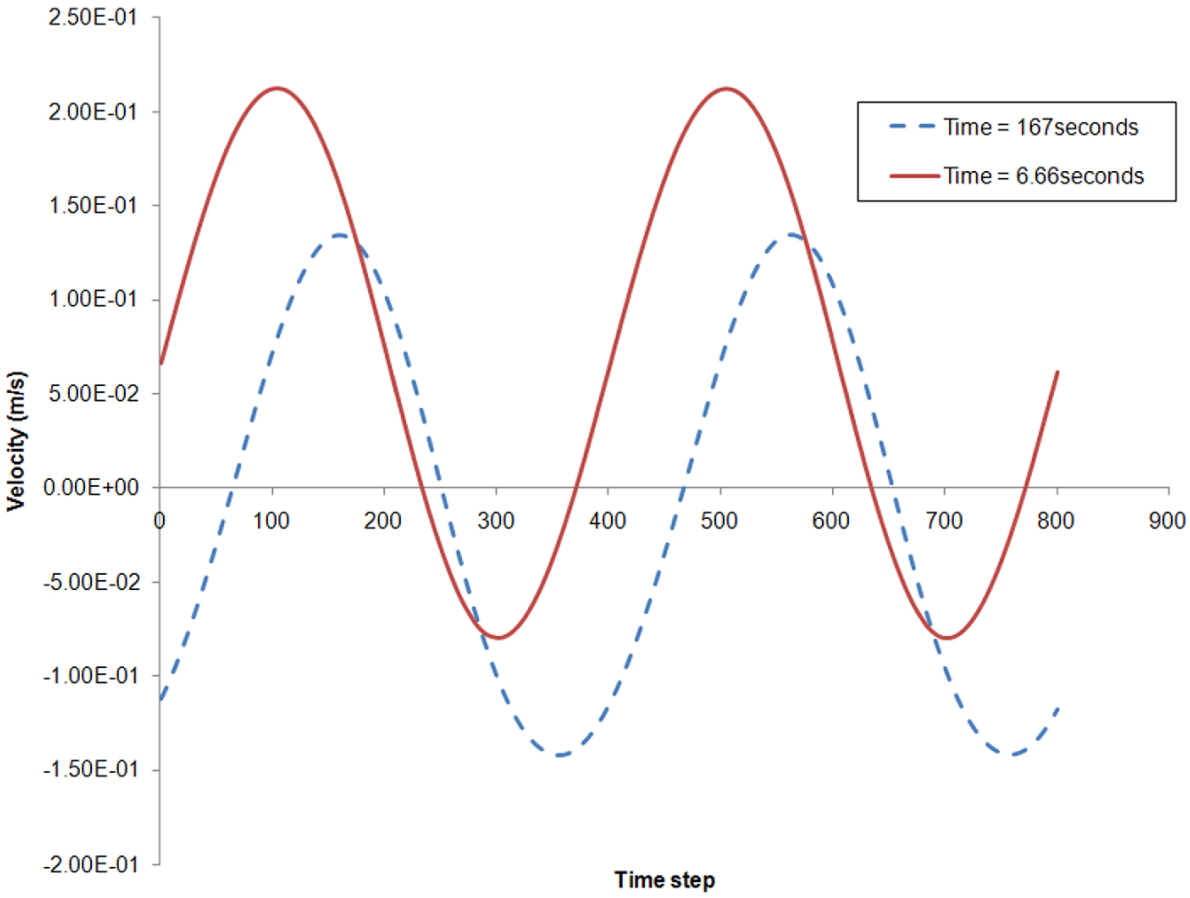
2.50E-01
2.00E-01
1.50E-01
1.00E-01
5.00E-02
0.00E+00
-5.00E-02
-1.00E-01
-1.50E-01
-2.00E-01
Velocity (m/s)
0
100
200
300
400
500
600
700
800
900
Time step
Time = 167seconds
Time = 6.66seconds

Figure 9:

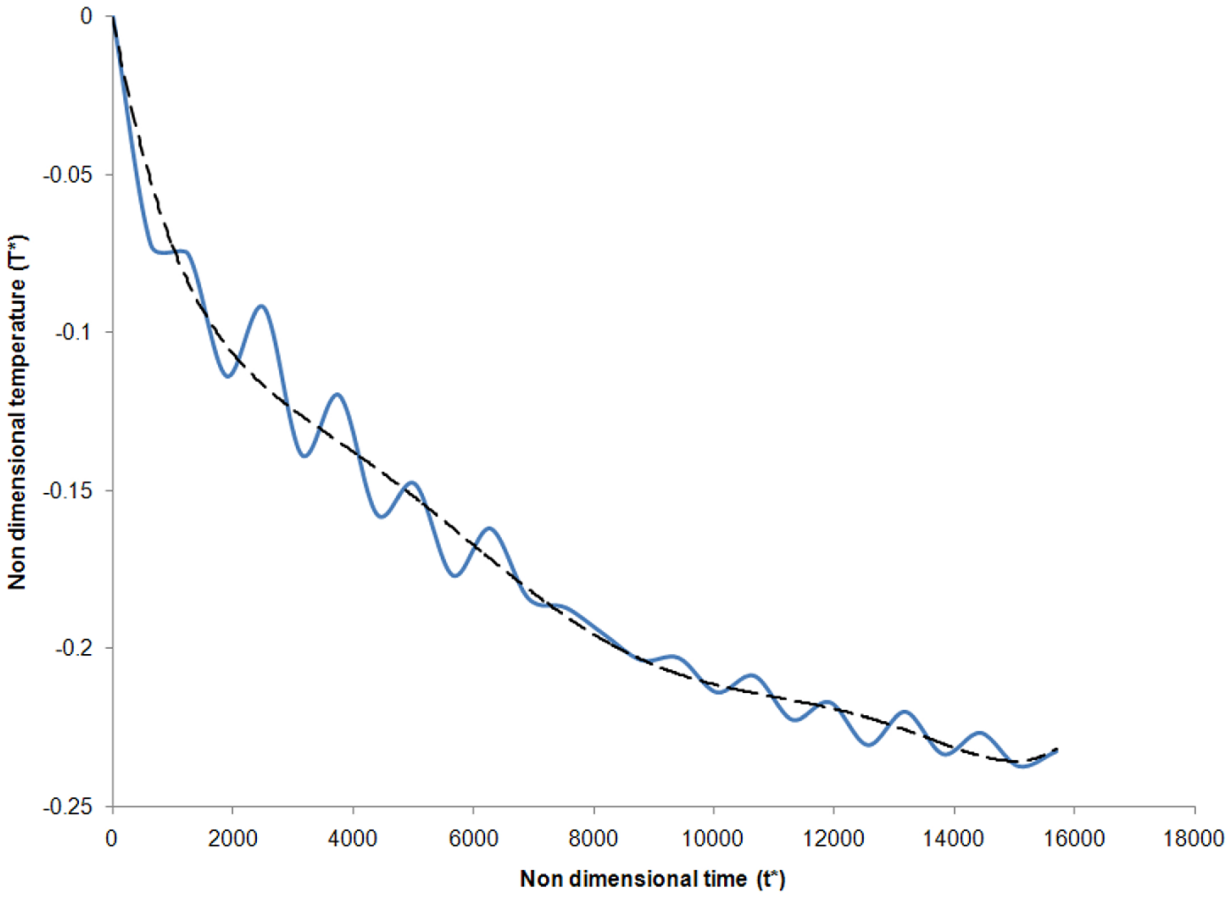
0
-0.05
-0.1
-0.15
-0.2
-0.25
Non dimensional temperature (T*)
0
2000
4000
6000
8000
10000
12000
14000
16000
18000
Non dimensional time (t*)

Figure 10:

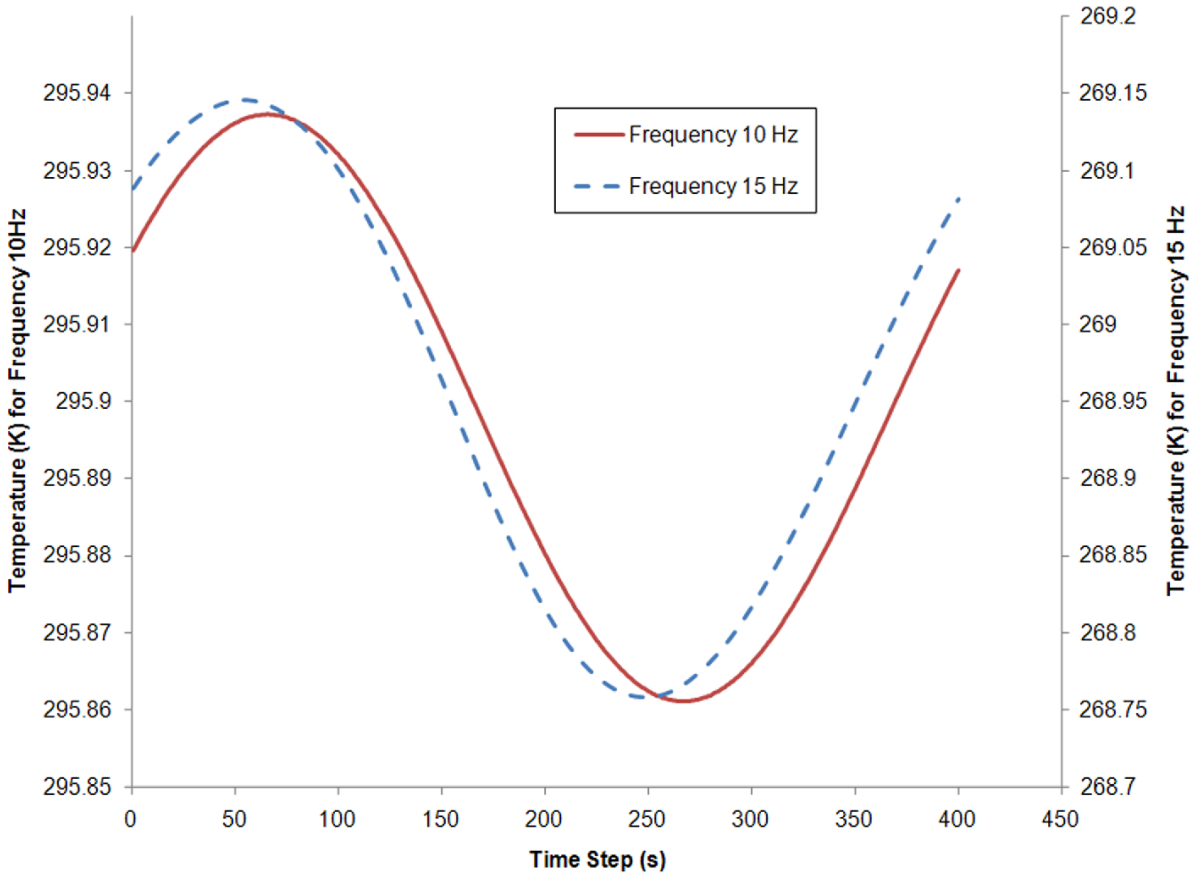
Frequency 10 Hz
Frequency 15 Hz
Temperature (K) for Frequency 10Hz
Temperature (K) for Frequency 15 Hz
Time Step (s)
295.94
295.93
295.92
295.91
295.9
295.89
295.88
295.87
295.86
295.85
269.2
269.15
269.1
269.05
269
268.95
268.9
268.85
268.8
268.75
268.7
0
50
100
150
200
250
300
350
400
450

Figure 11:

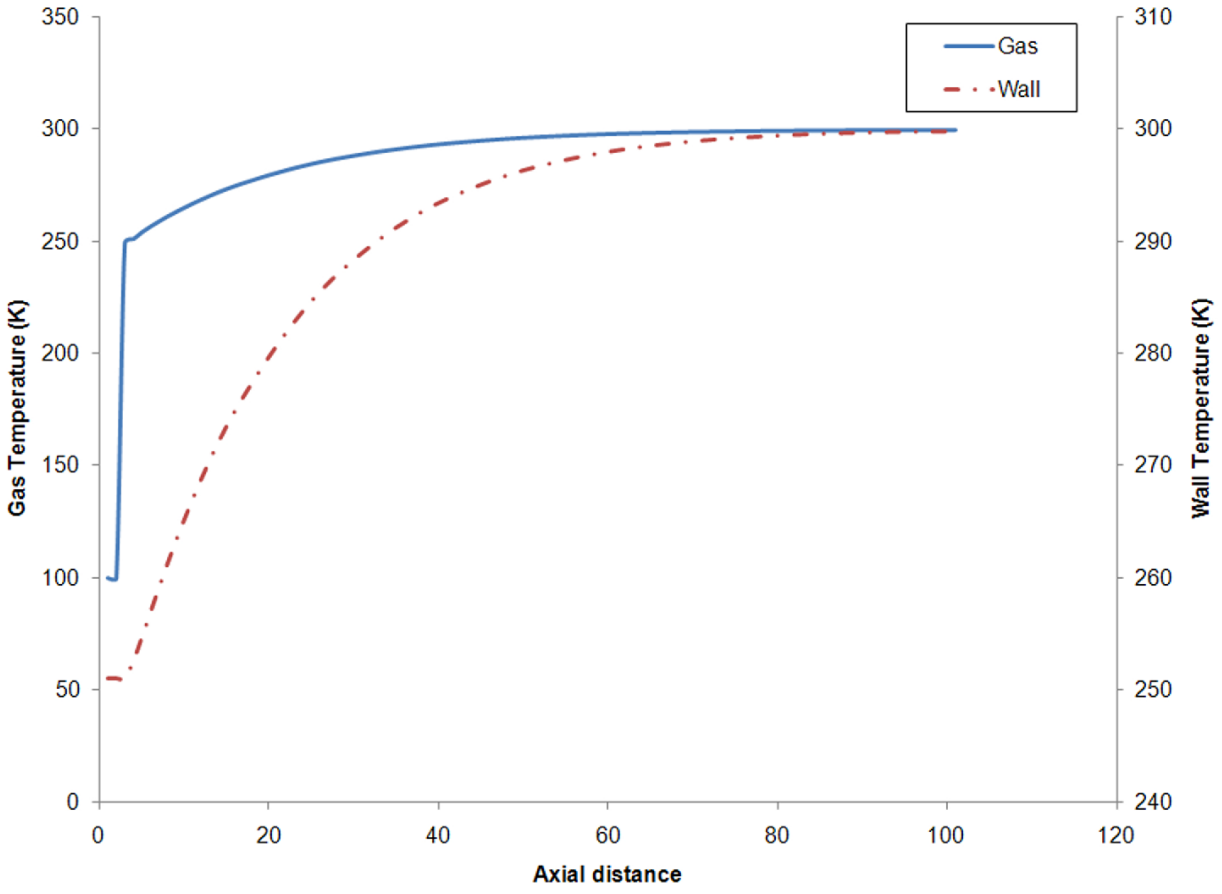
Gas
Wall
Gas Temperature (K)
Wall Temperature (K)
Axial distance
350
300
250
200
150
100
50
0
310
300
290
280
270
260
250
240
0
20
40
60
80
100
120

Figure 12:

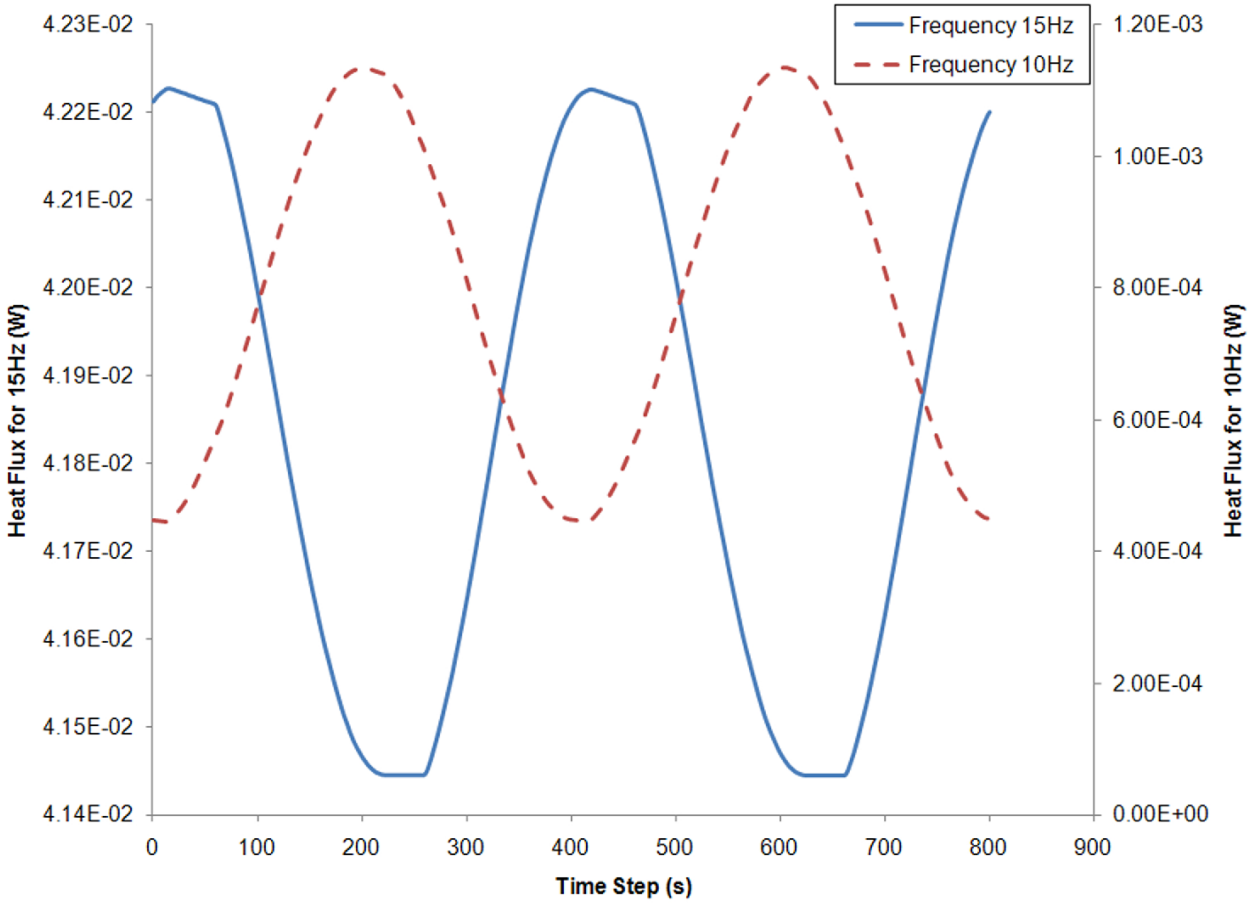
Frequency 15Hz
Frequency 10Hz
Heat Flux for 15Hz (W)
Heat Flux for 10Hz (W)
Time Step (s)
4.23E-02
4.22E-02
4.21E-02
4.20E-02
4.19E-02
4.18E-02
4.17E-02
4.16E-02
4.15E-02
4.14E-02
1.20E-03
1.00E-03
8.00E-04
6.00E-04
4.00E-04
2.00E-04
0.00E+00
0
100
200
300
400
500
600
700
800
900

Figure 13:

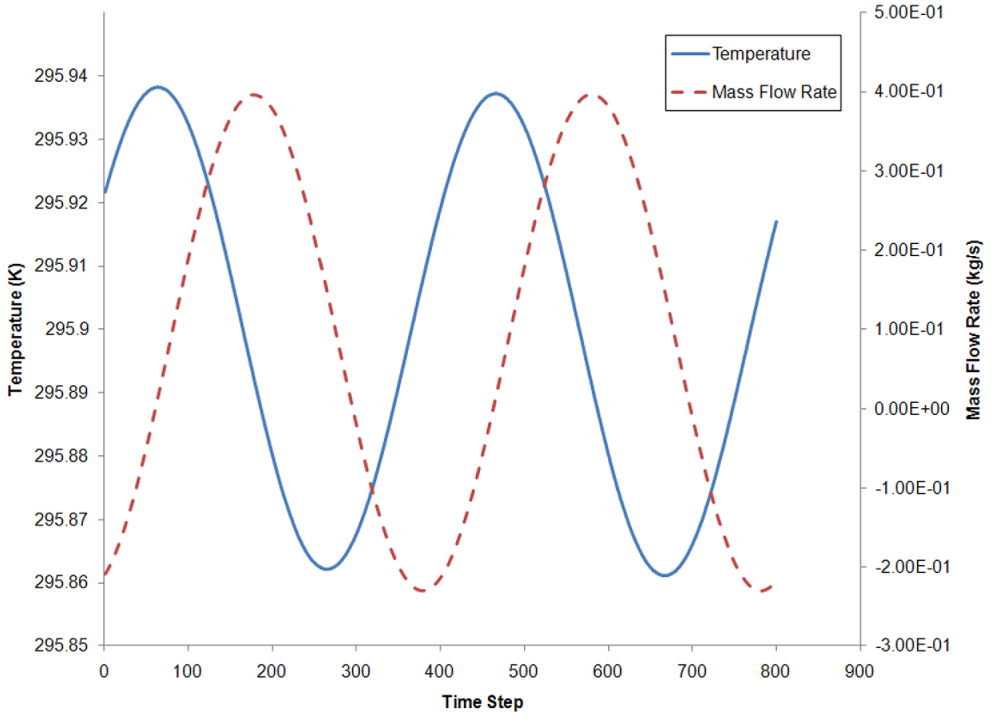
Temperature
Mass Flow Rate
Temperature (K)
Mass Flow Rate (kg/s)
Time Step
295.94
295.93
295.92
295.91
295.9
295.89
295.88
295.87
295.86
295.85
5.00E-01
4.00E-01
3.00E-01
2.00E-01
1.00E-01
0.00E+00
-1.00E-01
-2.00E-01
-3.00E-01
0
100
200
300
400
500
600
700
800
900

(a)

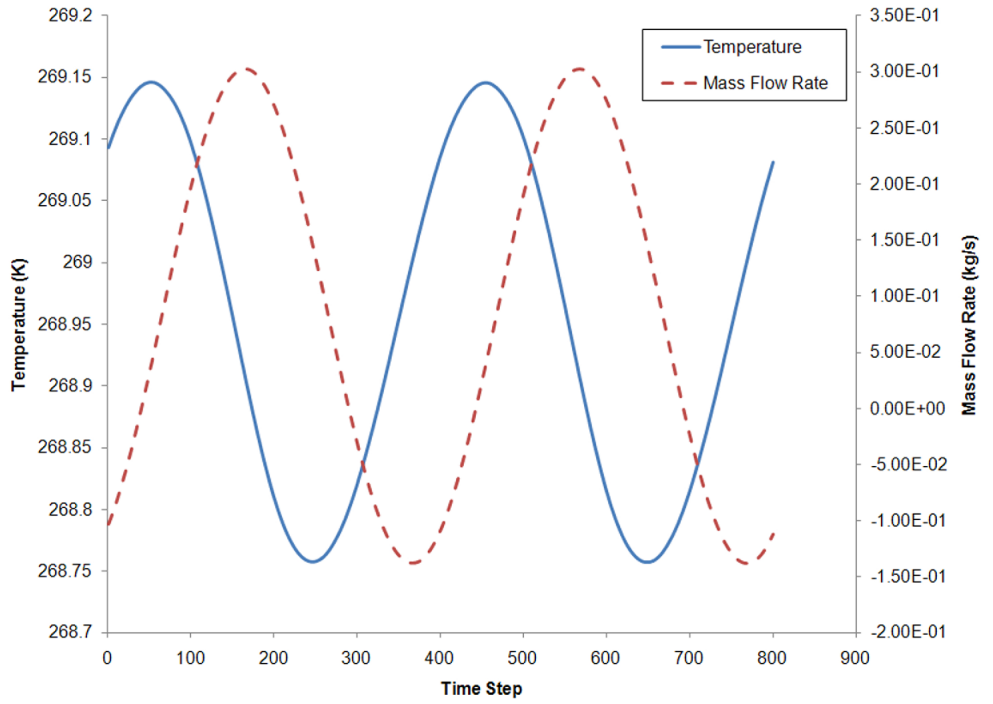
Temperature
Mass Flow Rate
Temperature (K)
Mass Flow Rate (kg/s)
Time Step
269.2
269.15
269.1
269.05
269
268.95
268.9
268.85
268.8
268.75
268.7
3.50E-01
3.00E-01
2.50E-01
2.00E-01
1.50E-01
1.00E-01
5.00E-02
0.00E+00
-5.00E-02
-1.00E-01
-1.50E-01
-2.00E-01
0
100
200
300
400
500
600
700
800
900

(b)

Figure 14: